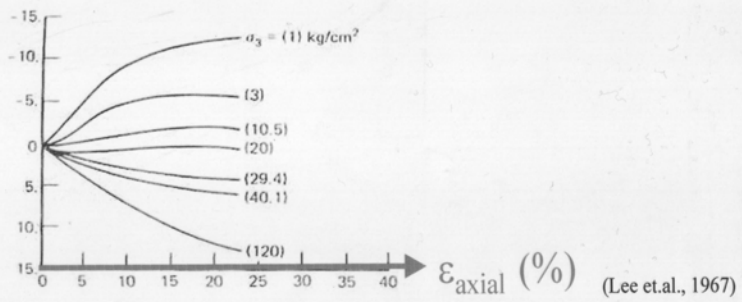
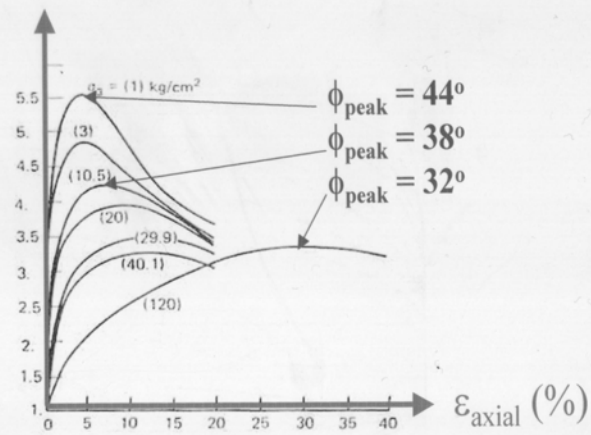


Razón de tensiones
 σ_1/σ_3

Arena de Sacramento
 $e_{\text{inicial}} = 0.61$

Deformación volumétrica
 $\varepsilon_v (\%)$



(Lee et.al., 1967)

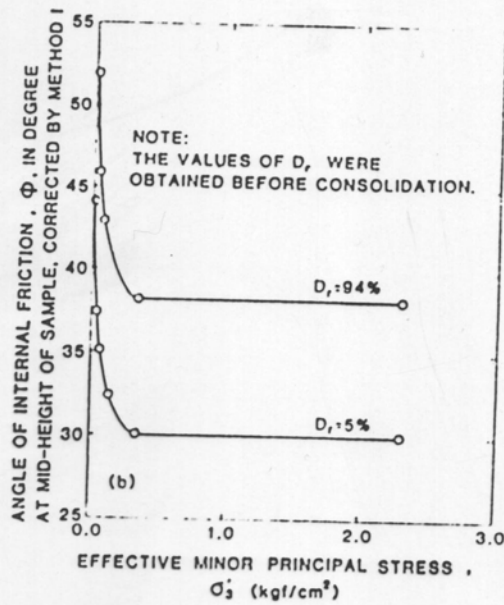
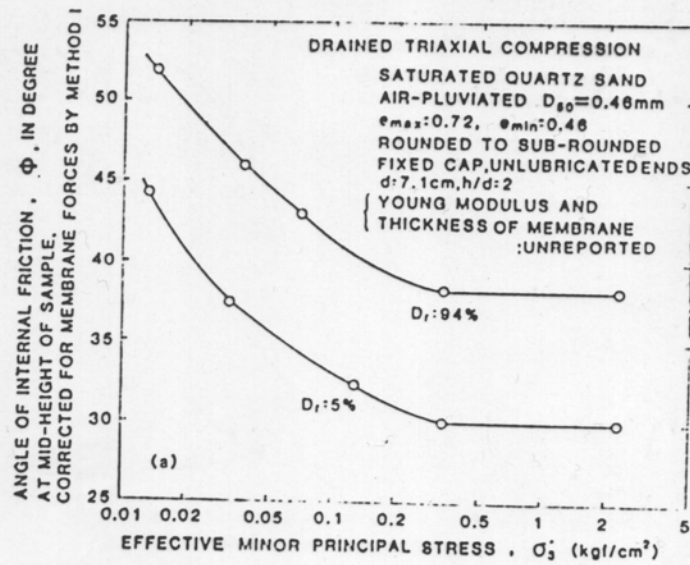


Fig. 1. Change of angle of internal friction by the change of effective minor principal stress in triaxial compression test (reproduced from Ponce and Bell, 1971) (1kgf/cm²=98kN/m²)

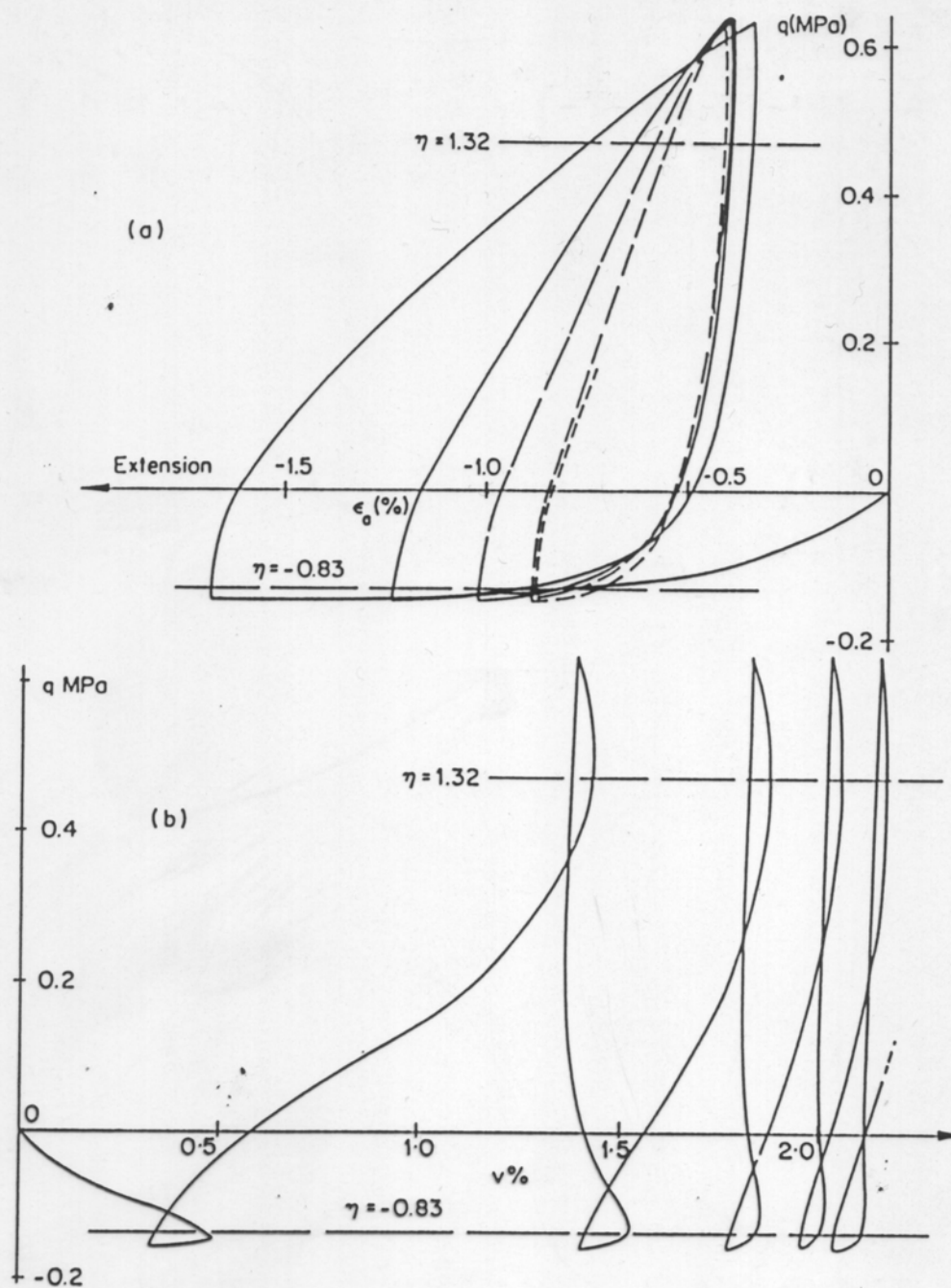


Figure 20.21 Cyclic triaxial drained compression-extension test on medium dense Fontainebleau sand (after Habib and Luong²⁹). Initial $D_r = 62\%$; confining pressure $\sigma_r = 200 \text{ kN/m}^2$

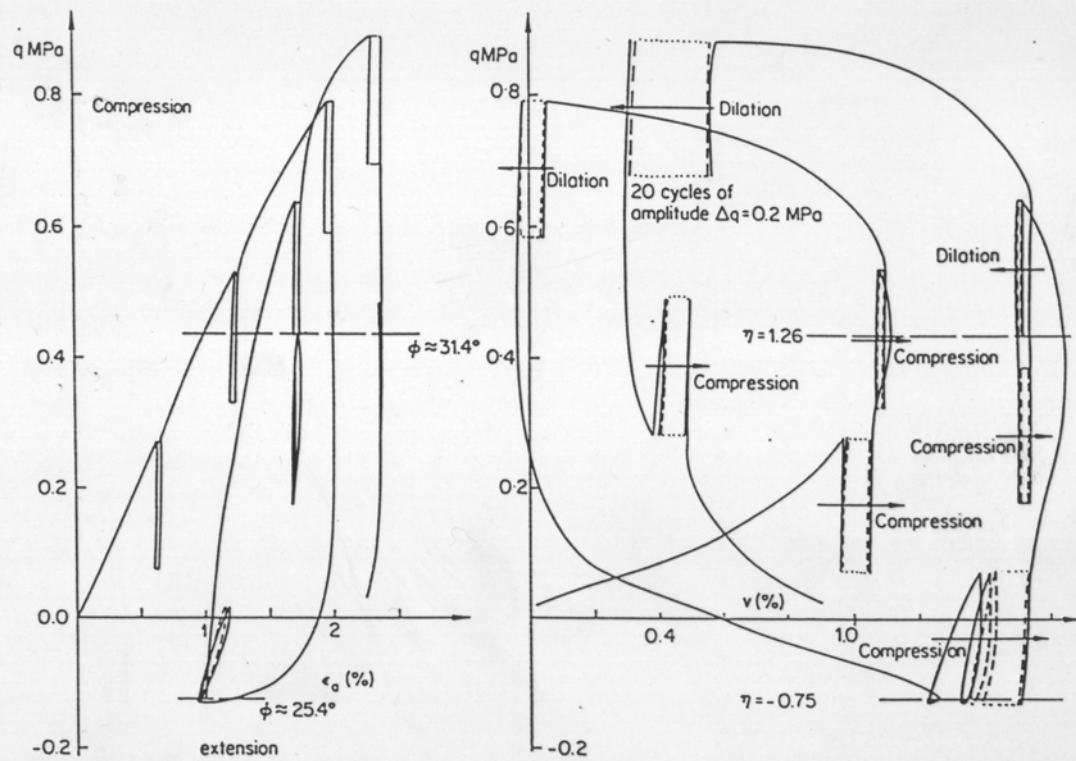


Figure 20.22 Compression or expansion observed in small cycles of load within large cycle of triaxial drained compression-extension test on medium dense Fontainebleau sand (after Habib and Luong²⁹). Initial $D_r = 64\%$; confining pressure $\sigma_r = 200 \text{ kN/m}^2$

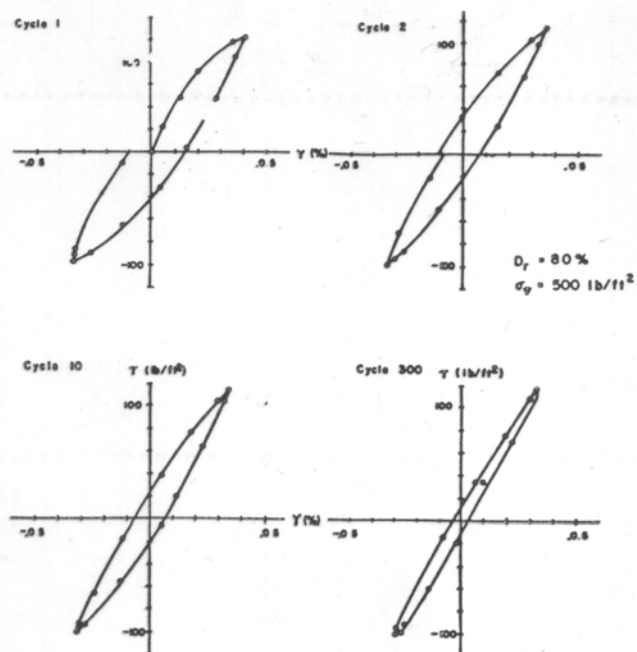


Fig. 19. Variación de la respuesta tensión-deformación con el número de ciclo, (Silver et al., 1969).

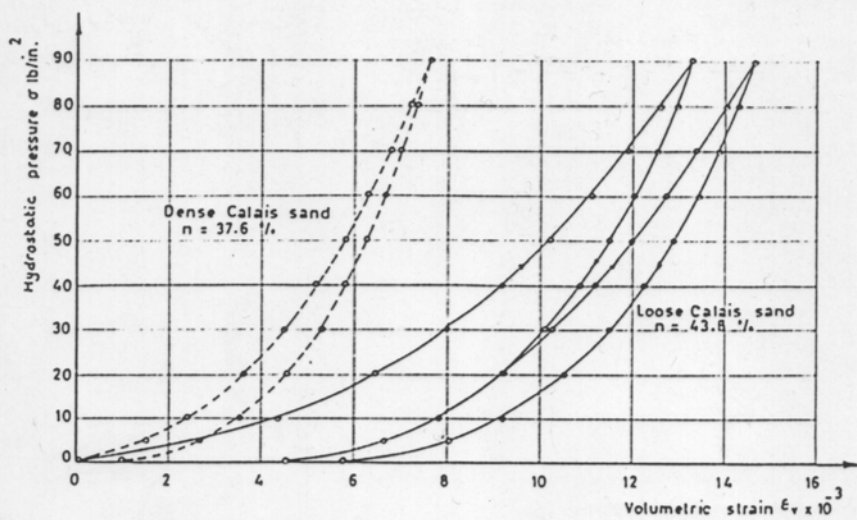


FIG. 6. Relations between volumetric strain and applied hydrostatic pressure—cycles of loading and unloading.

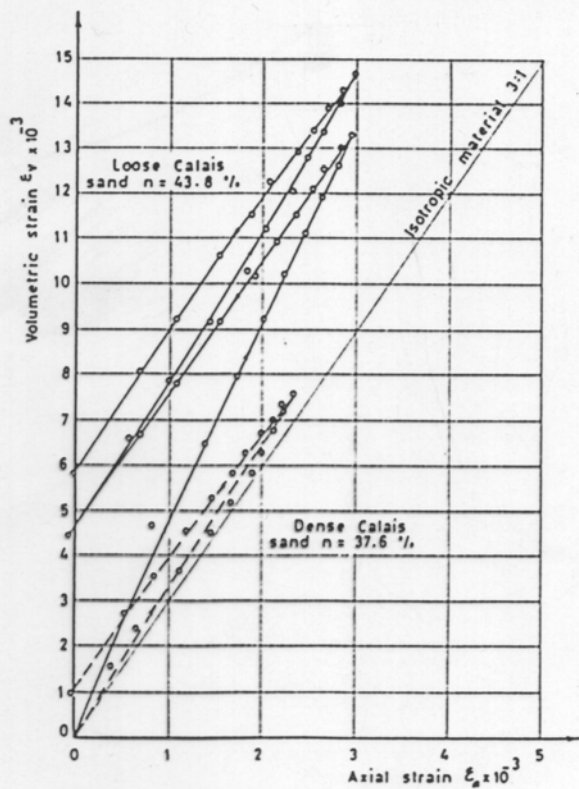
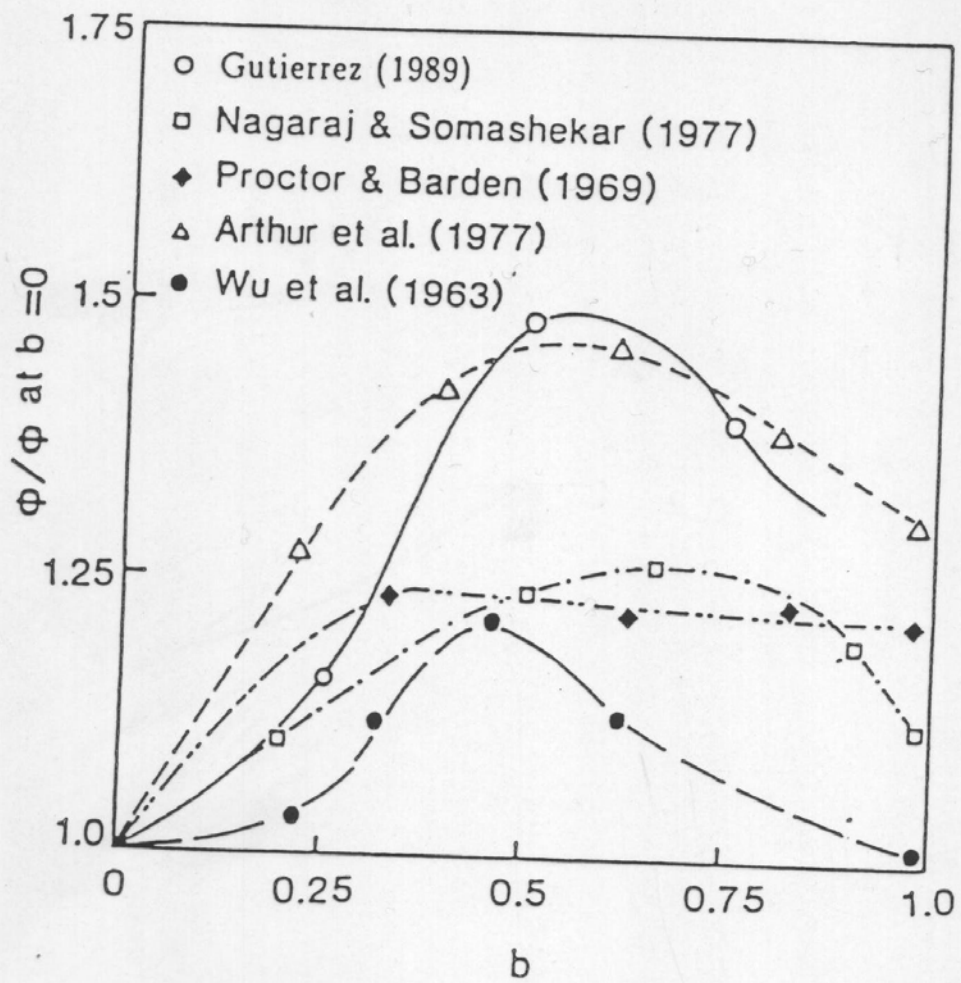
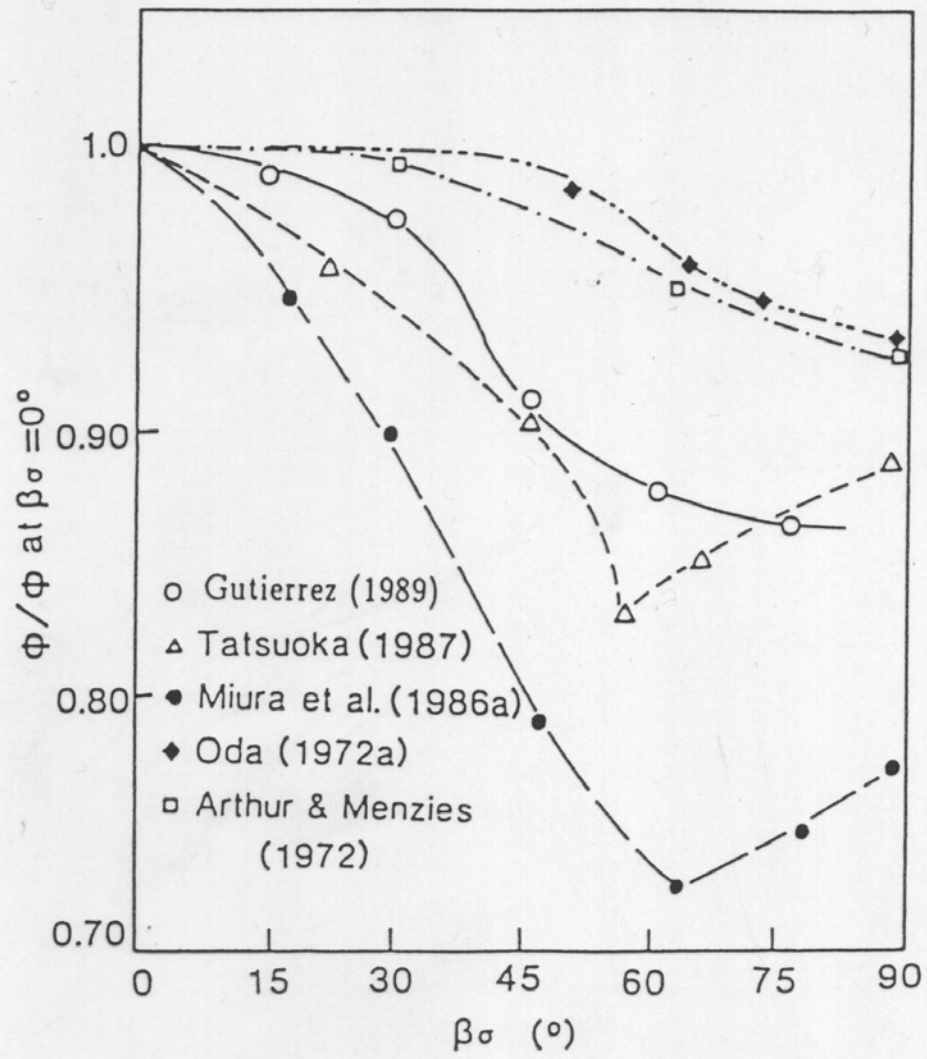


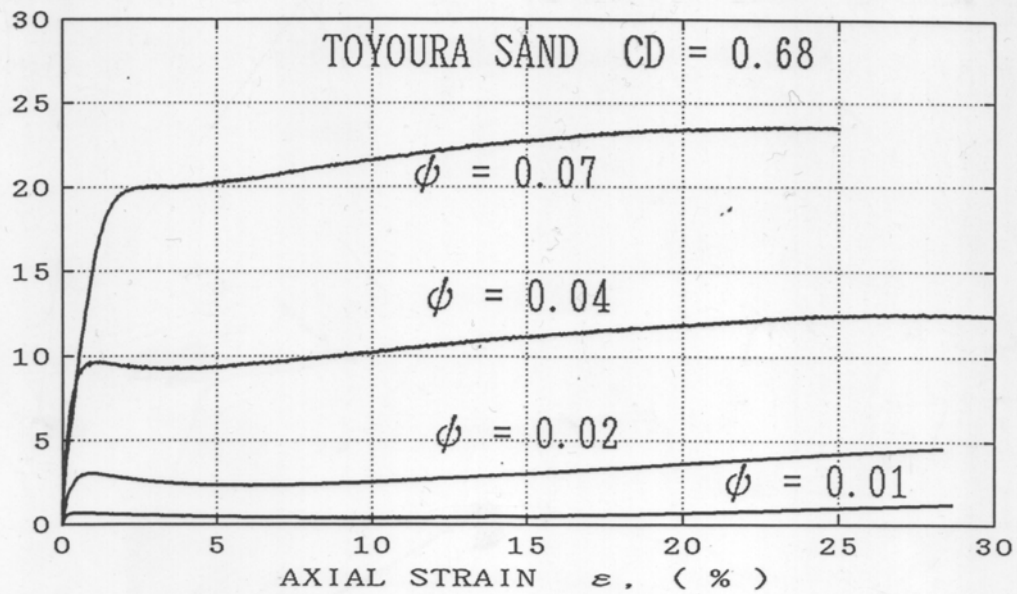
FIG. 7. Relations between volumetric and axial strains—cycles of loading and unloading.





$$q = \sigma_1 - \sigma_3$$

$$(kgf/cm^2)$$



$$q = \sigma_1 - \sigma_3$$

$$(kgf/cm^2)$$

